Characterization of mechanosynthesized $Bi_{1-x}Sm_xFeO_3$ samples unencumbered by secondary phases or compositional inhomogeneity

Eva Gil-González[a,b*], Antonio Perejón[a,b,c*], Pedro E. Sánchez-Jiménez[a], Michael A. Hayward[b], José M. Criado[a], María J. Sayagués[a], Luis A. Pérez-Maqueda[a]

[a] *Instituto de Ciencia de Materiales de Sevilla (C.S.I.C.-Univ. Sevilla). C. Américo Vespucio 49, Sevilla 41092. Spain*
[b] *Department of Chemistry, Inorganic Chemistry Laboratory, University of Oxford, South Parks Road, Oxford OX1 3QR,United Kingdom*
[c] *Departamento de Química Inorgánica, Facultad de Química, Universidad de Sevilla, Sevilla 41071, Spain*

Corresponding Authors

*E mail: antonio.perejon@icmse.csic.es. Tel. (+34) 95 448 95 00. Fax (+34) 95 446 01 65.
*E mail: eva.gil@icmse.csic.es. Tel. (+34) 95 448 95 00. Fax (+34) 95 446 01 65.

Characterization of mechanosynthesized $Bi_{1-x}Sm_xFeO_3$ samples unencumbered by secondary phases or compositional inhomogeneity

Eva Gil-González[a,b*], Antonio Perejón[a,b,c*], Pedro E. Sánchez-Jiménez[a], Michael A. Hayward[b], José M. Criado[a], María J. Sayagués[a], Luis A. Pérez-Maqueda[a]

[a] *Instituto de Ciencia de Materiales de Sevilla (C.S.I.C.-Univ. Sevilla). C. Américo Vespucio 49, Sevilla 41092. Spain*
[b] *Department of Chemistry, Inorganic Chemistry Laboratory, University of Oxford, South Parks Road, Oxford OX1 3QR, United Kingdom*
[c] *Departamento de Química Inorgánica, Facultad de Química, Universidad de Sevilla, Sevilla 41071, Spain*

Abstract

High-quality samples, in terms of phase purity and dielectric properties, of composition $Bi_{1-x}Sm_xFeO_3$ ($0.05 \leq x \leq 0.20$) have for the first time been prepared by mechanosynthesis. Close inspection of the powder diffraction data, analysis via Rietveld refinement and TEM microscopy demonstrates that the $Bi_{1-x}Sm_xFeO_3$ samples contain only perovskite phases. Additionally, by a combination of Rietveld analysis, TEM, DSC, temperature-dependent XRD and permittivity data a tentative phase diagram has been proposed where the high temperature paraelectric phase Pnma has been confirmed for samarium substituted $BiFeO_3$. Regarding the physical properties, the samples resulted to be electrically homogenous and highly insulating at room temperature, suggesting that other sources of conductivity, such as mixed valence of Fe associated with possible oxygen non-stoichiometry, have been avoided during the samples synthesis. In spite of the high quality of the samples, the dielectric and magnetic behaviour of the $Bi_{1-x}Sm_xFeO_3$ samples change only modestly on Sm substitution, with neither a great change in the resistivity or remnant magnetisation of Sm substituted samples in comparison with $BiFeO_3$.

Keywords: Sm substituted BiFeO3; multiferroics; mechanochemical processing; structure identification; phase transitions

1. Introduction

Multiferroic materials - those which exhibit at least two of the so-called "ferroic" properties: ferroelectricity, ferromagnetism and ferroelasticity [1-3] – offer many new opportunities to prepare novel devices which exploit the coupling between these different polarizations. This is particularly true of coupled magnetoelectric multiferroic materials. One of the most widely studied magnetoelectric materials is the perovskite oxide $BiFeO_3$, because it is one of the few known materials which exhibit both a spontaneous magnetic polarization and a spontaneous electric polarization at room temperature. Specifically $BiFeO_3$ adopts a polar, rhombohedrally distorted perovskite structure (space group R3c) at room temperature and remains ferroelectric at temperatures up to 830 ºC. Furthermore $BiFeO_3$ adopts a canted antiferromagnetically ordered state at temperatures up to 360 ºC [4-8]. These relatively high transition temperatures make $BiFeO_3$ a candidate for use in novel spintronic applications such as multistate memory devices or magnetoelectric sensors [9].

Despite the obvious advantages offered by the high magnetic and ferroelectric ordering temperatures of $BiFeO_3$, there are a number of obstacles which need to be overcome before this material can be utilized in devices. The most notable of these is the small electrical polarization observed in bulk ceramic samples which tends to be accompanied by high leakage currents, hampering the ferroelectric switching [10]. Furthermore the modest spontaneous magnetization observed for bulk samples at room temperature couples only weakly to the electrical polarization due to the presence of a symmetry averaging spin cycloid [5]. These non-ideal physical properties can be caused by, or exacerbated by, a further obstacle to the implementation of $BiFeO_3$ in devices: the difficulty in preparing high-quality, single-phase stoichiometric samples. Under the high-temperature 'ceramic' synthesis conditions typically used to prepare $BiFeO_3$, Bi_2O_3 is much more volatile than Fe_2O_3. As a result samples prepared in this manner tend to be bismuth deficient [7, 11-12]. Low levels of bismuth deficiency can result in the formation of cation vacancies which can act as p-type doping centres, enhancing the conductivity of the samples [13]. At higher levels of bismuth deficiency, iron-rich secondary phases such as $Bi_2Fe_4O_9$ form, which also degrade desired physical behaviour [14-16].

One of the most popular approaches to address both the non-optimal physical behaviour and challenging synthesis of $BiFeO_3$, has been to partially substitute the Bi^{3+} 'A-cations' with rare earth cations in order to both optimize the electric and magnetic behaviour of the material and

simplify the preparation of high quality samples [17-25]. However a brief survey of the many reports describing the crystal structure and/or physical behaviour of substituted $Bi_{1-x}RE_xFeO_3$ materials reveals a bewildering array of complex, often contradictory information.

The variability in the results of A-site substitution of $BiFeO_3$ can again be attributed to the difficulties associated with sample preparation. The high volatility of bismuth requires low synthesis temperatures to ensure stoichiometric samples are prepared, however the low rates of solid-state diffusion at these temperatures seriously hamper attempts to synthesise samples with homogeneous substituent distributions suggesting that some A-cation substituted $Bi_{1-x}RE_xFeO_3$ phases are more challenging to prepare than $BiFeO_3$ itself [26-29].

Considering the samarium substituted $BiFeO_3$ series, several authors have reported that bismuth substitution by samarium in $BiFeO_3$ ($Bi_{1-x}Sm_xFeO_3$) remarkable enhanced the properties of bulk ceramic, prepared by several different synthesis methods [21, 26, 30-32]. However, there is no consensus regarding the crystal structure and physical properties of the bulk ceramics as a function of the samarium content. Thus, it has been reported that the polar R3c structure of $BiFeO_3$ is retained for samarium content in the range $0 \leq x \leq 0.15$ [31], but in other works it has been concluded that the main phase for $x = 0.15$ can be indexed in the Pbam space group [23, 26, 33]. On the other hand, other authors consider that at this composition two phases, R3c and Pbnm, coexist [13]. Moreover, discrepancies are not only found in the crystal structures at different compositions but also in the phase transition temperatures. Thus, different transition temperatures are reported for samples with the same composition. These discrepancies may be due to the different synthesis methods employed, which play an extremely important role in the resulting properties of the materials, as stated above [28]. Additionally, many of them normally give rise to routine impurities, mainly $Bi_2Fe_4O_9$ and $Bi_{25}FeO_{39}$ [21, 30, 33-36].

Mechanochemical approaches appear to be well suited to addressing the synthetic challenges associated with the preparation of $Bi_{1-x}RE_xFeO_3$ phases [37-44]. By mixing reagents via vigorous mechanical agitation at 'ambient' temperature, samples with highly homogenous elemental distributions can be achieved without Bi_2O_3 evaporation. The precursor phases can then be rapidly sintered over time periods of just a few minutes to yield highly crystalline, chemically homogenous, stoichiometric samples.

Here we describe a case study of the $Bi_{1-x}Sm_xFeO_3$ $0.05 < x < 0.2$ compositional range to demonstrate the utility of mechanosynthesis approaches for $Bi_{1-x}RE_xFeO_3$ materials and to

get a true view of the effects of substitution on the physical behaviour of $BiFeO_3$ unencumbered by the presence of secondary phases or compositional inhomogeneity.

2. Materials and methods

Sample Preparation.

Samples of composition $Bi_{1-x}Sm_xFeO_3$ (x = 0.05, 0.1, 0.125, 0.15, 0.175, 0.2) were prepared by mechanosynthesis. Suitable stoichiometric ratios of Bi_2O_3 (10 μm, 99.9% purity), Fe_2O_3 (<5 μm, ≥99% purity) and Sm_2O_3 (99.9% purity) were mechanically milled using a modified Pulverisette 7 (Fritsch, Idar-Oberstein, Germany) planetary mill. Samples were milled under 7 bars of oxygen (to avoid bismuth reduction) for time periods described latter in the text, using hardened steal jars (80 cm^3 volume) and balls (9 balls, 15 mm diameter) with a powder:ball mass ratio of 1:20 and a spinning rate of the supporting disc of 700 rpm.

After milling, the $Bi_{1-x}Sm_xFeO_3$ powders obtained were pressed into cylindrical pellets (without binder) of approximately 6 mm diameter, 2 mm thickness, by applying a uniaxial pressure of 0.93 GPa. The pellets were then sintered at 900 ºC in air, with no annealing time to prevent sample decomposition [12], employing heating and cooling rates of 10 ºC min^{-1}. Taking into account that Bi_2O_3 reacts with Fe_2O_3 and Sm_2O_3 during the mechanosynthesis to form the $Bi_{1-x}Sm_xFeO_3$ phases, the samples can be sintered at 900 ºC without melting or volatilization of Bi_2O_3. The density of the pellets was measured by the Archimedes' method, using distilled water at room temperature as the immersion liquid.

Sample Characterisation.

X-ray powder diffraction patterns were collected using a Panalytical X'Pert Pro diffractometer (CuKα radiation) equipped with an X'Celerator detector and a graphite diffracted beam monochromator. Rietveld refinements were carried out with FullProf software. Temperature-dependent X-ray powder diffraction patterns were recorded in a 100 cm^3 min^{-1} airflow using a Philips X'Pert Pro diffractometer equipped with a high-temperature Anton Par camera, using CuKα radiation and equipped with an X'Celerator detector and a graphite diffracted beam monochromator. Celref software was used to determine the lattice parameters at high temperature. Differential scanning calorimetry (DSC) curves were measured from -50 ºC to 400 ºC using a DSC Instrument (Q200, TA Instruments, Crawley,

UK), and also using a simultaneous TG/DSC Instrument (Q600 SDT, TA Instruments, Crawley, UK) in the temperature range from 400 ºC to 850 ºC. The samples were placed in open alumina pans and measurements were performed at a heating rate of 10 ºC min^{-1} and under an airflow of 100 cm^3 min^{-1}. The microstructure of the samples was analysed by transmission electron microscopy (TEM) and scanning electron microscopy (SEM). High resolution transmission electron microscopy measurements (HRTEM) were performed using a 200 kV TEM Philips CM 200 microscope with B$_6$La filament. SEM micrographs of the sintered pellets were obtained using a Hitachi S-4800 microscope, equipped with an energy dispersive X-ray spectrometer (EDX). The pellets were thermally etched for 30 min at 90% of the sintering temperature (810 ºC) to reveal the grain boundaries. Dielectric measurements were carried out as a function of temperature using a 4263B LCR meter. Impedance spectroscopy measurements were performed taking into account the blank capacitance of the sample holder and the overall pellet geometry, whose opposite faces were previously Au sputter-coated using an Emitech K550 Sputter Telstar (Barcelona, Spain). The impedance measurements were taken in a Newtons4th Ltd impedance analyser (Loughborough, UK) over the frequency range from 100 Hz to 1 MHz, with ac measuring voltage of 0.1 V. The samples are highly insulating at room temperature, with resistivity values between 10^{17}-10^{12} Ωcm. Upon increasing temperature, the resistivity decreases so that impedance measurements can be performed from 300 ºC. A maximum temperature of 400 ºC was selected to avoid degradation of the gold coating. Magnetic data were collected using a Quantum Design MPMS SQUID magnetometer from powder samples.

3. Results

Crystallographic characterisation.

Samples of composition Bi$_{1-x}$Sm$_x$FeO$_3$ (0.05 < x < 0.2) were prepared by direct mechanosynthesis. The reaction of the pristine oxides to form products with the general formula Bi$_{1-x}$Sm$_x$FeO$_3$ was followed by X-ray diffraction. As an example, XRD patterns at periodic intervals of the milling process are shown in the Supplementary Material, Figure S1, for composition x = 0.10. Figure 1 shows the X-ray powder diffraction data collected from the Bi$_{1-x}$Sm$_x$FeO$_3$ samples prior to sintering, along with the milling time required to complete the reaction. It can be seen that the milling time required to complete the reaction increased with samarium content. The broad diffraction peaks observed in Figure 1 are attributable to

the nanometric crystallite size of the samples. These broad diffraction features of the unsintered samples make it hard to extract detailed crystallographic information, nevertheless it is clear that the diffraction profile of the x = 0.2 sample is significantly different from those of the other compositions.
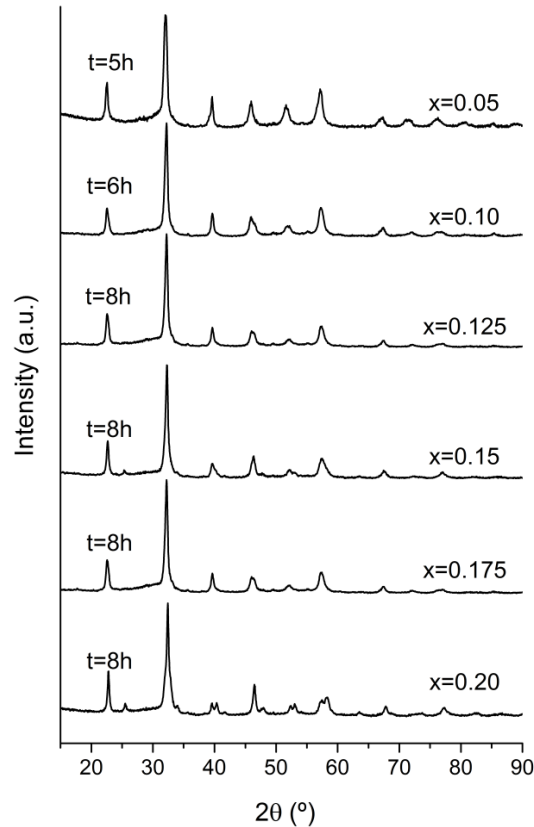

Figure 1. XRD patterns of powders of composition $Bi_{1-x}Sm_xFeO_3$ obtained after milling suitable stoichiometric ratios of the single oxides in oxygen (7 bar) for the indicated milling times.

Figure 2 shows expanded sections of the XRD data collected in the range 20º < 2θ < 45º from $Bi_{1-x}Sm_xFeO_3$ samples after sintering at 900 ºC. The achieved relative pellet densities were above 93% in all the samples. Close examination reveals dramatic changes in the powder diffraction data as a function of samarium content. The x = 0.05 and x = 0.10 samples can be simply indexed using a rhombohedral unit cell (space group R3c), typical of $BiFeO_3$ at room temperature. As the samarium content increases above x = 0.125 there are significant changes in the XRD patterns, such that the data can no longer be indexed by a single rhombohedral unit cell, indicating that a change in structure has occurred.
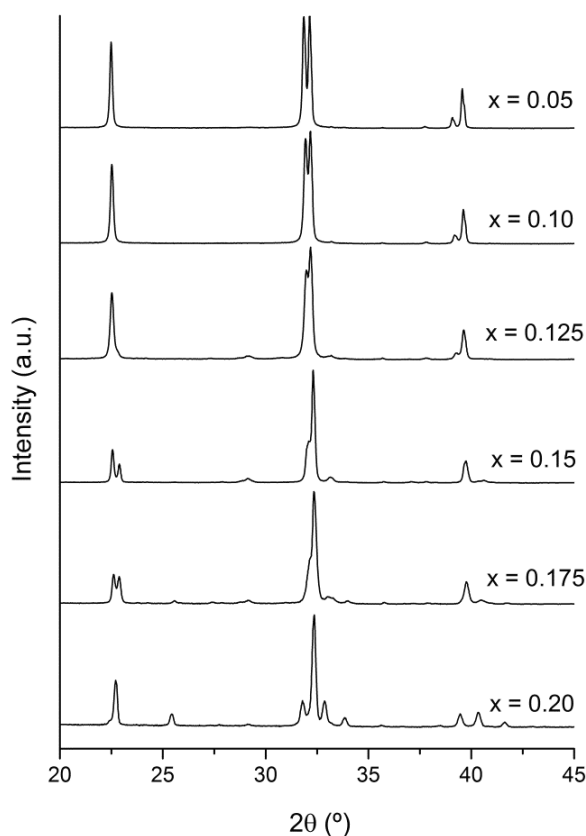
Figure 2. XRD patterns of the mechanosynthesized samples of composition $Bi_{1-x}Sm_xFeO_3$ obtained after sintering at 900 ºC.

The structural evolution of the $Bi_{1-x}Sm_xFeO_3$ system was analysed by the Rietveld method. As noted above, data from the x = 0.05 and x = 0.10 samples can be successfully fitted using a rhombohedral R3c structure (Table 1) with good reliability factors (See Supplementary Material, Figures S2-S3). Both samples appear to be phase-pure, although very small features can be observed that may correspond to extremely small amounts of secondary phases that, therefore, cannot be identified and quantified.

Attempts were made to index the diffraction data from x ≥ 0.125 samples using a number of different unit cells and space groups (*R3c, Pnma, Pbam, Amm2, C221, Imma, P2mm, Pmc2₁, Pn2₁a*). Data collected from the x = 0.15 sample could be readily indexed using an orthorhombic unit cell, in the centrosymmetric space group *Pbam* (Figure 3). Refinement of a crystallographic model constructed in this unit cell gave a good fit to the data (Table 1) indicating that the XRD pattern of $Bi_{0.85}Sm_{0.15}FeO_3$ does not present significant peaks corresponding to secondary phases. The same strategy was employed to index and refine the

diffraction data from the x = 0.20 sample (See Supplementary Material, Figure S4), with the best results obtained using an orthorhombic unit cell in space group Pnma (Table 1).

Diffraction data collected from the x = 0.125 and x = 0.175 samples could not be indexed by single unit cells, however these data could be fitted well using a structural model containing two phases. Fits to the data from the x = 0.125 sample demonstrate that it is a mixture of an R3c phase (72%) and a Pbam phase (28%) at this composition (See Supplementary Material, Figure S5). Similarly fits to the diffraction data collected from the x = 0.175 composition demonstrate that it is a mixture of a Pbam phase (74%) and Pnma phase (26%) (Table 1 and Supplementary Material, Figure S6).

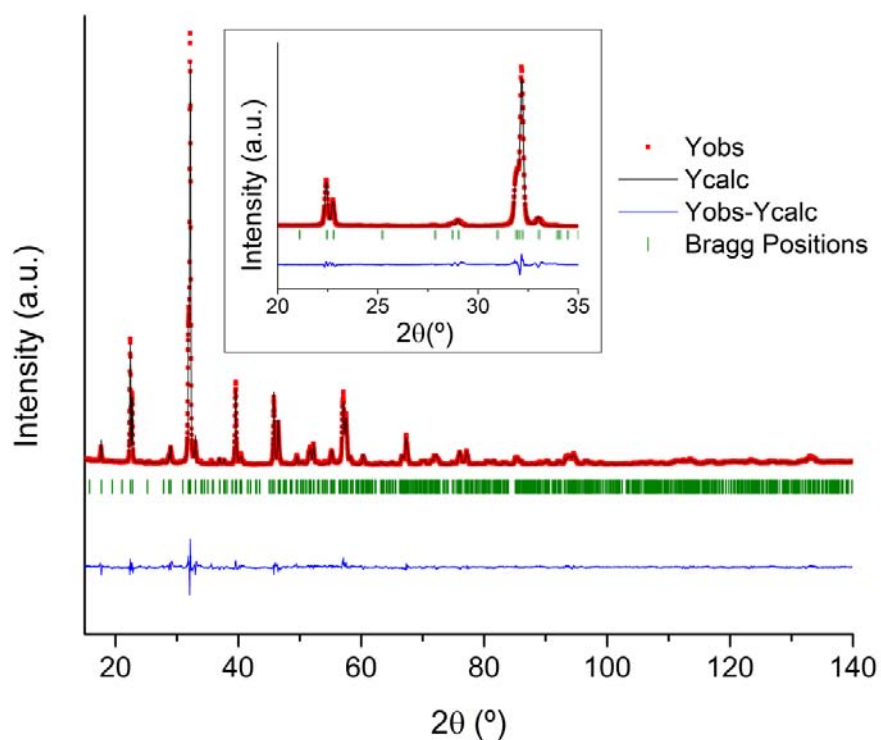Figure 3. XRD pattern of $Bi_{0.85}Sm_{0.15}FeO_3$ obtained after 8 h milling, and sintered at 900ºC (dots). The solid line corresponds to the fit from the Rietveld refinement. Bragg reflections for *Pbam* space group are indicated by sticks. The inset shows an expanded section of the diffractogram in the region from 20º to 35º 2θ.

Table 1. Rietveld refinements and structural parameters obtained from the XRD patterns of the samples $Bi_{0.95}Sm_{0.05}FeO_3$, $Bi_{0.90}Sm_{0.10}FeO_3$, $Bi_{0.875}Sm_{0.125}FeO_3$, $Bi_{0.85}Sm_{0.15}FeO_3$, $Bi_{0.825}Sm_{0.175}FeO_3$ and $Bi_{0.80}Sm_{0.20}FeO_3$, sintered at 900 ºC.

Sample	$Bi_{0.95}Sm_{0.05}FeO_3$	$Bi_{0.90}Sm_{0.10}FeO_3$	$Bi_{0.875}Sm_{0.125}FeO_3$	
Space group	R3c	R3c (100% w/w)	R3c (72 $\pm$ 2% w/w)	Pbam (28 $\pm$ 2% w/w)
a (Å)	5.5742(1)	5.5695(1)	5.5655(10)	5.5887(21)
b (Å)	5.5742(2)	5.5695(1)	5.5655 (10)	11.2213(13)
c (Å)	13.8352(1)	13.7989(3)	13.7744(28)	7.8044(10)
Volume (Å³)	372.283(3)	370.594(4)	369.493(2)	489.434(5)
Atomic positions				
Bi (1)	0.00, 0.00, 0.00	0.00, 0.00, 0.00	0.00, 0.00, 0.00	0.7197(3), 0.1242(4), 0.00
Bi (2)	-	-	-	0.7038(5), 0.1336(2), 0.50
Sm (1)	0.00, 0.00, 0.00	0.00, 0.00, 0.00	0.00, 0.00, 0.00	0.7197(1), 0.1242(2), 0.00
Sm (2)	-	-	-	0.7038(2), 0.1336(5), 0.50
Fe	0.00, 0.00, 0.2219(4)	0.00, 0.00, 0.2246(3)	0.00, 0.00, 0.2239(5)	0.2264(6), 0.11658(5), 0.2375(4)
O (1)	0.4391(3), 0.0059(2), 0.9544(4)	0.4449(4), 0.0105(2), 0.9553(1)	0.4453(2), 0.0214(6), 0.9510(1)	0.2890(2), 0.1690(1), 0.00
O (2)	-	-	-	0.3190(3), 0.1090(4), 0.50
O (3)	-	-	-	0.0240(5), 0.2630(7), 0.2870(4)
O (4)	-	-	-	0.00, 0.50, 0.2050(3)
O (5)	-	-	-	0.00, 0.00, 0.2400(2)
Confidence factors				
R_{wp}	9.36	13.0	10.7	
χ^2	4.14	4.23	4.61	
Sample	$Bi_{0.85}Sm_{0.15}FeO_3$	$Bi_{0.825}Sm_{0.175}FeO_3$		$Bi_{0.80}Sm_{0.20}FeO_3$
Space group	Pbam (100% w/w)	Pbam (74 $\pm$1 % w/w)	Pnma (26 $\pm$1 % w/w)	Pnma (100% w/w)
a (Å)	5.5887(1)	5.5792(2)	5.6216(2)	5.6216(1)
b (Å)	11.2208(3)	11.1887(4)	7.8141(5)	7.8141(2)
c (Å)	7.8039(2)	7.7985(3)	5.4429(2)	5.4429(1)
Volume (Å3)	489.434(3)	486.846(5)	239.098(6)	239.10(3)
Atomic positions				
Bi (1)	0.7163(2), 0.1232(1), 0.00	0.7209(6), 0.1245(4), 0.00	0.0255(2), 0.2500, 0.988(3)	0.0457(2), 0.25,0.9960(5)
Bi (2)	0.7017(5), 0.1341(4), 0.50	0.7053(3), 0.1343(2), 0.50	-	-
Sm (1)	0.7163(6), 0.1232(3), 0.00	0.7209(1), 0.1245(4), 0.00	0.0255(3), 0.2500, 0.9883(5)	0.0457(4), 0.25,0.9960(6)
Sm (2)	0.7017(2), 0.1341(1), 0.50	0.7053(3), 0.1343(6), 0.50	-	-
Fe	0.2344(5), 0.1177(4), 0.2490(3)	0.2402(5), 0.1223(2), 0.2567(3)	0.00, 0.00, 0.50(2)	0.00, 0.00,0.50(4)
O (1)	0.2448(3), 0.1836(2), 0.00	0.2286(7), 0.1936(3), 0.00	0.4853(3), 0.2500, 0.0764(4)	0.4817(1), 0.25,0.0889(3)
O (2)	0.3000(1), 0.1222(5), 0.50	0.3024(3), 0.1429(4), 0.50	0.2095(6), 0.5340(3), 0.2148(2)	0.2896(2), 0.0409(5),0.7128(6)
O (3)	0.0240(2), 0.2639(3), 0.2243(4)	0.0240(2), 0.2662(1), 0.50	-	-
O (4)	0.00, 0.50, 0.1852(1)	0.00, 0.50, 0.1625(6)	-	-
O (5)	0.00, 0.00, 0.2209(5)	0.50, 0.00,0.2021(4)	-	-
Confidence factors				
R_{wp}	11.0	13.0		16.5
χ^2	5.38	5.38		2.60

Microstructural and chemical characterisation.

The microstructure of the samples was analysed by means of electron microscopy. Representative results for composition x = 0.10 are presented in Figure 4. The sample is formed by agglomerated crystalline domains that oscillate between 100 and 300 nm as can

be seen in Figure 4a. A high resolution micrograph of one of these domains is presented in Figure 4b, where the (1 1 0) interplanar distances, corresponding to the symmetry R3c of the analysed phase, have been measured (marked in the HR image). Due to the size of the crystalline domains, many of the obtained diffraction patterns are formed by rings, although some larger domains could be oriented like the one depicted in Figure 4c along the [2 0 1] zone axis.

Samples $x = 0.15$ and $x = 0.20$ showed smaller crystalline domain than $x = 0.10$. The electron diffraction (ED) patterns are in agreement with the X-ray diffraction data. The ED patterns and TEM images for these compositions are presented in the Supplementary Material, Figures S7-S8.
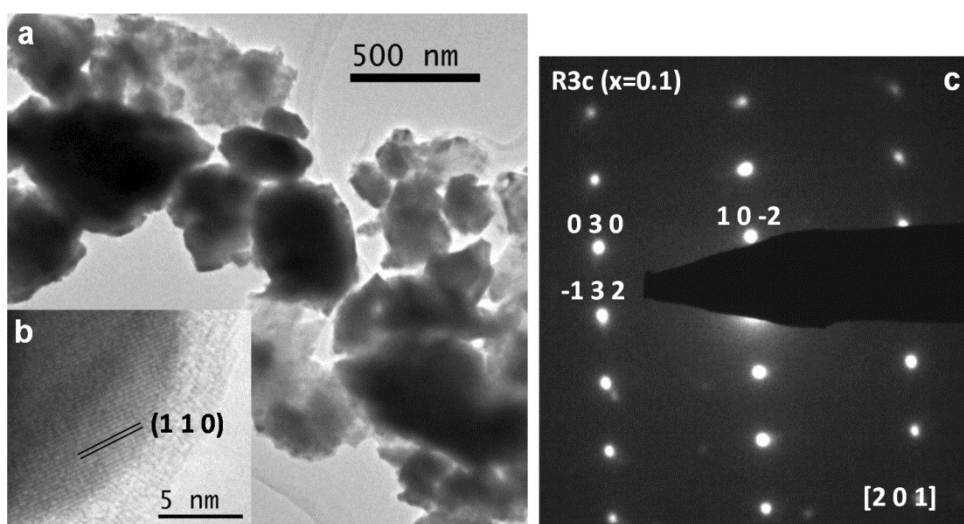

Figure 4. a) TEM micrograph, b) HR image and c) ED pattern along [2 0 1] for the sample with composition x = 0.10.

The microstructure of the pellets was studied by SEM. Figure 5 shows the micrographs of the samples prepared by mechanosynthesis and sintered at 900 ºC for compositions x = 0.05, 0.10, 0.15 and 0.20. Basically, the microstructure of the samples is composed by densely packed grains with a quite wide distribution size. It can be clearly observed that the grains size decreases with the amount of substituent. Table 2 lists the elemental composition of the samples, determined by the semiquantitative analysis of the EDX spectra. As it may be observed, the experimental results are consistent with the expected compositions and

therefore the materials maintain the nominal composition after the synthesis process. Slight differences are observed, which can be attributed to the intrinsic errors of the EDX method.
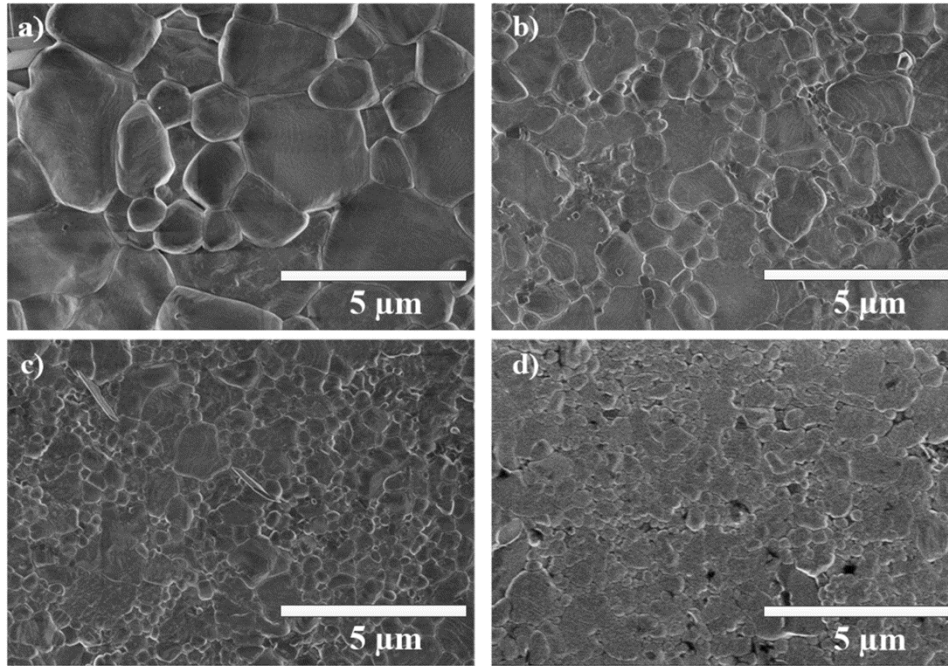

Figure 5. SEM micrographs of the pellets obtained after milling and sintering at 900°C: a) $Bi_{0.95}Sm_{0.05}FeO_3$, b) $Bi_{0.90}Sm_{0.10}FeO_3$, c) $Bi_{0.85}Sm_{0.15}FeO_3$, d) $Bi_{0.80}Sm_{0.20}FeO_3$.

Table 2. Elemental composition of the samples prepared by mechanosynthesis and sintered at 900°C, determined by the semiquantitative analysis of EDX spectra.

		Experimental atomic composition (%)		
Sample	Theoretical atomic composition Fe/Sm/Bi (%)	Fe	Sm	Bi
$Bi_{0.95}Sm_{0.05}FeO_3$	50.0/2.5/47.5	51.0 ± 1.9	2.2 ± 0.7	46.8 ± 1.5
$Bi_{0.90}Sm_{0.10}FeO_3$	50.0/5.0/45.0	49.2 ± 1.7	5.0 ± 0.5	45.8 ± 1.5
$Bi_{0.85}Sm_{0.15}FeO_3$	50.0/7.5/42.5	49.4 ± 1.5	7.6 ± 0.7	43.0 ± 1.7
$Bi_{0.80}Sm_{0.20}FeO_3$	50.0/10.0/40.0	50.7 ± 1.8	9.9 ± 0.6	39.4 ± 1.6

Temperature dependant behaviour.

Figures 6a and 6b show the DSC data from sintered samples of $Bi_{1-x}Sm_xFeO_3$ in the temperature ranges $-50 < T/°C < 400$ °C and $400 < T/°C < 850$ °C, respectively. Data from all $Bi_{1-x}Sm_xFeO_3$ samples exhibit an endothermic peak at $T \sim 370$ °C which corresponds to the onset of magnetic order ($T_N = 360$ °C for $BiFeO_3$). In addition data from all samples, with the exception of the $x = 0.2$ sample, show an additional endothermic peak which appears at a temperature which declines with increasing samarium content. In order to establish the nature of the phase transitions associated with these latter endothermic features, XRD patterns were

collected in air from $Bi_{0.95}Sm_{0.05}FeO_3$, $Bi_{0.90}Sm_{0.10}FeO_3$, $Bi_{0.875}Sm_{0.125}FeO_3$, $Bi_{0.85}Sm_{0.15}FeO_3$ and $Bi_{0.825}Sm_{0.175}FeO_3$ at temperatures close to these DSC endothermic peaks.
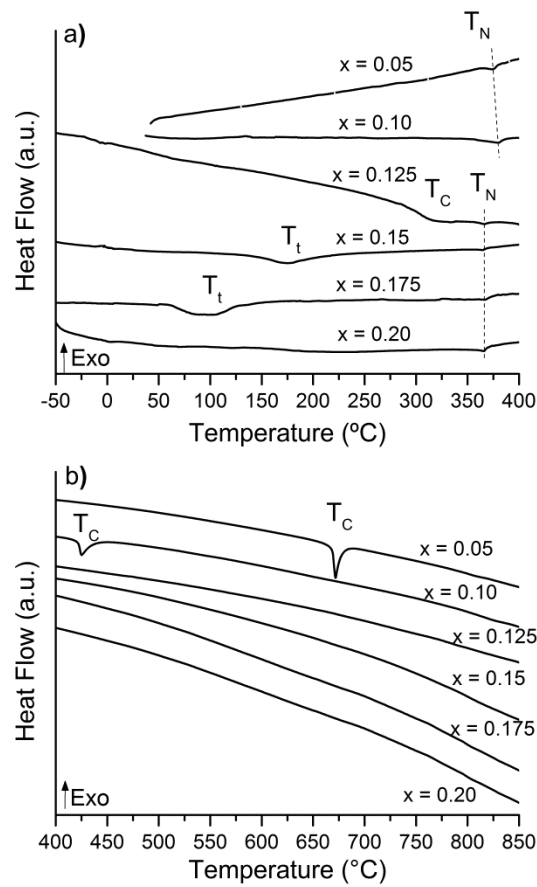

Figure 6. DSC traces of the mechanosynthetized samples of composition $Bi_{1-x}Sm_xFeO_3$, registered after sintering at 900ºC. The dashed lines linking T_N are guides to the eye. T_N, T_C and T_t denote the Néel, Curie and phase transition temperatures, respectively.

Figures 7a and 7b show a series of X-ray powder diffraction data collected as a function of temperature, in the range $20º < 2\theta < 45º$, from the $x = 0.05$ and $x = 0.10$ samples, respectively. These data reveal that the endothermic peaks seen in the DSC data collected from the samples (Figure 6b) at 671ºC and 424 ºC, respectively, correspond to structural phase transitions from the polar R3c structure at low temperature to the centrosymmetric Pnma structure at high temperature, in a directly analogous manner to the phase transition observed for non-substituted $BiFeO_3$ at its Curie temperature (830 ºC) [45]. Thus, we can identify the Curie temperatures of the $x = 0.05$ and $x = 0.10$ samples as 671ºC and 424 ºC, respectively. Figure 7c shows a series of X-ray powder diffraction data collected as a function of temperature from the $x = 0.15$ sample, confirming that the peak observed at 175ºC in the DSC data corresponds to a phase transition from a Pbam structure at low

temperature to a Pnma structure at high temperature, being both space groups centrosymmetric.

Analogous variable temperature X-ray powder diffraction data collected from the x = 0.125 and x = 0.175 samples at temperatures around those at which the DSC peaks were observed for these two phases (314 ºC for x = 0.125; 107 ºC for x = 0.175) show a steady evolution which corresponds to a change from the two phase mixtures observed at low temperature (R3c+Pbam for x = 0.125; Pbam+Pnma for x = 0.175) to a Pnma structure at high temperature (See Supplementary Material, Figure S9). These data are summarized in Table 3, along with the lattice parameters of the high-temperature Pnma phases, determined by use of the Celref software.
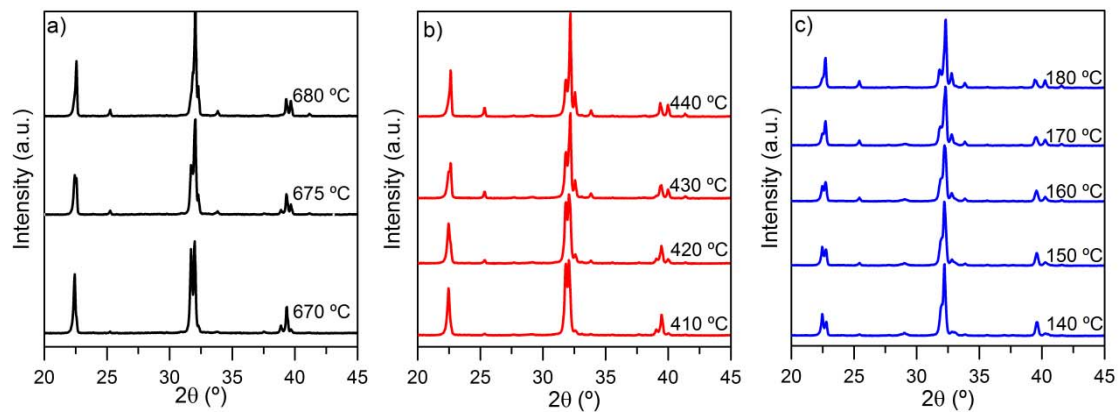

Figure 7. In situ XRD patterns of the samples at different temperatures: a) $Bi_{0.95}Sm_{0.05}FeO_3$, b) $Bi_{0.90}Sm_{0.10}FeO_3$, c) $Bi_{0.85}Sm_{0.15}FeO_3$.

Table 3. Phase transition temperatures and cell parameters at 800ºC, 500ºC, 400ºC, 200ºC and 150ºC for x = 0.05, x = 0.10, x=0.125, x = 0.15 and x=0.175 compositions, respectively.

Sample	T (ºC)	Phase transition	Cell parameters
$Bi_{0.95}Sm_{0.05}FeO_3$	671 ºC	R3c→Pnma	T=800ºC
			a=5.6237(3), b=7.9166(2), c=5.5709(4), α=β=γ=90º
$Bi_{0.90}Sm_{0.10}FeO_3$	424 ºC	R3c→Pnma	T=500ºC
			a=5.6338(5), b=7.8677(5), c=5.5264(2), α=β=γ=90º
$Bi_{0.875}Sm_{0.125}FeO_3$	314 ºC	R3c+Pbam→Pnma	T=400ºC
			a=5.6376(4), b=7.8714(3), c=5.5199(5), α=β=γ=90º
$Bi_{0.85}Sm_{0.15}FeO_3$	175 ºC	Pbam→Pnma	T=200ºC
			a=5.6323(3), b=7.8351(2), c=5.4884(2), α=β=γ=90º
$Bi_{0.825}Sm_{0.175}FeO_3$	107 ºC	Pbam+Pnma→Pnma	T=150ºC
			a=5.6243(5), b=7.8499(5), c=5.4755(4), α=β=γ=90º

Figure 8 shows relative permittivity data collected as a function of temperature, at a frequency of 100 KHz, from the x = 0.10, 0.125, 0.15 and 0.175 samples. The data from the 0.10 and 0.125 samples show maxima in the permittivity at 425 ºC and 315ºC, respectively which provide confirmation that the phase transitions in these samples at these temperatures correspond to transition from ferroelectric to paraelectric states. Likewise the lack of equivalent maxima in the permittivity's of the remaining samples are also consistent with the structural phase transitions described in Table 3.
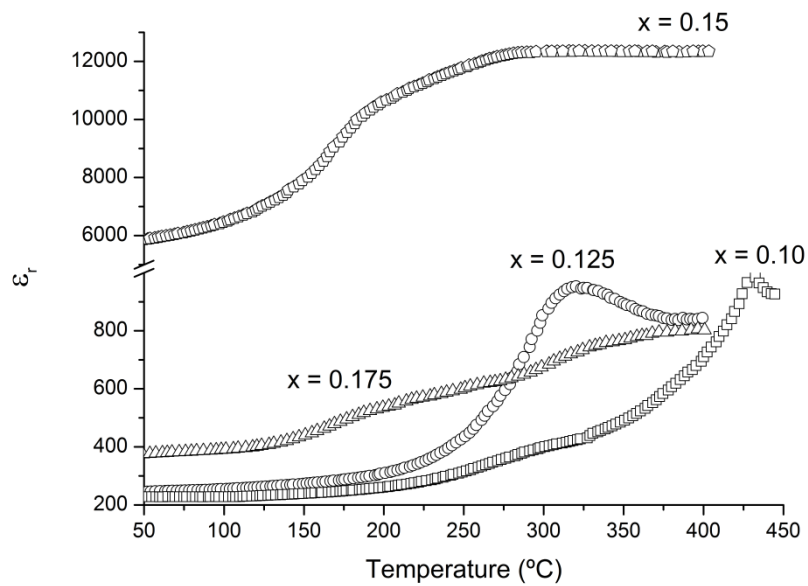

Figure 8. Temperature dependence of relative permittivity at a frequency of 100 KHz for x = 0.10, 0.125, 0.15 and 0.175 compositions.

The DSC, temperature-dependent DRX and permittivity data allow a tentative phase diagram of the $Bi_{1-x}Sm_xFeO_3$ system to be constructed as shown in Figure 9. It can be observed the composition dependence of T_C and T_N, together with the corresponding phase transition temperatures.
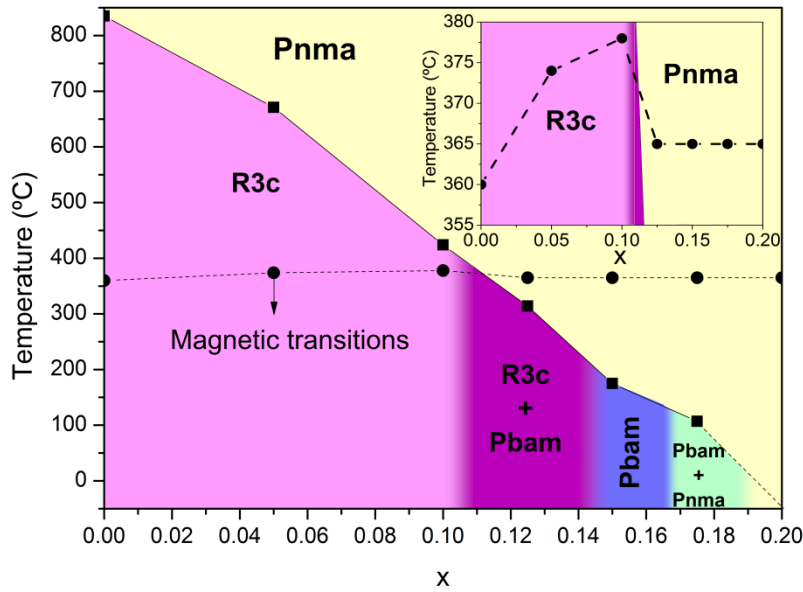
Figure 9. Tentative phase diagram for the system $Bi_{1-x}Sm_xFeO_3$. Néel (T_N), Curie (T_C) and phase transition (T_t) temperatures were taken from the DSC traces shown in Figure 6. The inset details the changes of T_N in the studied compositional range.

Physical behaviour.

The electrical behaviour of the samples was also studied as a function of temperature by impedance spectroscopy. The samples were highly insulating at room temperature, presenting low conductivity from 300ºC. Figure 10 presents impedance data for x = 0.10 in the temperature range from 300ºC to 400ºC. The impedance complex plane plot (Figure 10a) shows distorted single arcs, from which the total resistance of the sample at each temperature is obtained as the intercept with the x axis. Figure 10b shows, as an example, the M'' and Z'' spectroscopic plots at 380ºC. Single broad peaks with slight displacement between them for the maxima frequency are obtained. Moreover, no additional peak is observed in the Z'' plot at lower frequency, which suggests that the samples are electrically homogenous. Figure 10c shows the capacitance data, which are composed by high-frequency plateaus that are followed by small increase in the C' values at low frequency. Conductivity plots present similar tendencies (Figure 10d), with plateaus at low frequency and dispersion at high frequency. These tendencies in both capacitance and conductivity plots may indicate a possible power law response [46]. Similar results were obtained for the other compositions (See Supplementary Material, Figure S10).
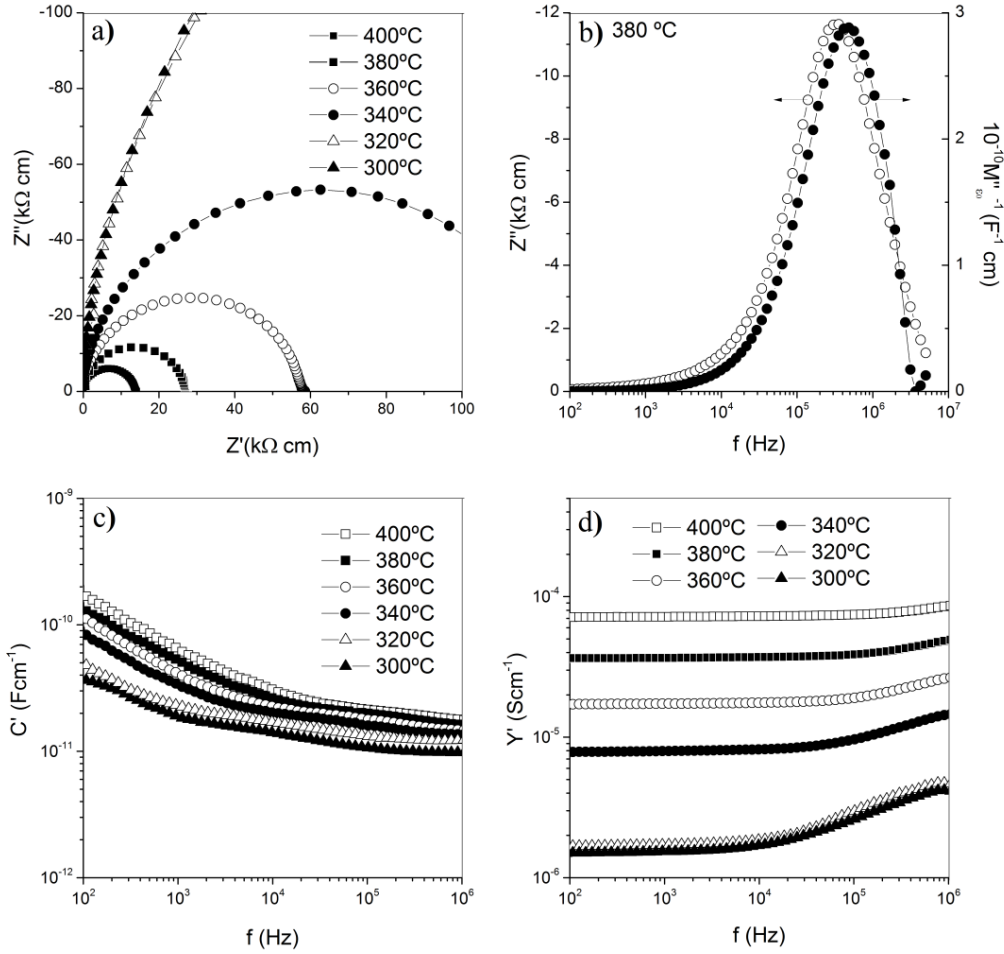
16

Figure 10. a) Impedance plots, b) Z″/M″ spectroscopic plots, and c) C′ and d) Y′ vs frequency for $Bi_{0.90}Sm_{0.10}FeO_3$ obtained after milling, and sintered at 900ºC.

The resistivity values obtained from the interception on the real Z' axes, in conventional Arrhenius format (log σ against the inverse of temperature, being σ the conductivity), are shown in Figure 11 for compositions x = 0.05, 0.10, 0.15 and 0.20. Extrapolating from this graph, the conductivity of the samples is small with resistivity values between 2×10^{17} and 1×10^{12} Ωcm at room temperature. These low conductivities suggest that other sources of conductivity, such as mixed valence of Fe associated with possible oxygen non-stoichiometry, have been avoided during the sample synthesis in contrast with the results presented by other authors, whose samples present high levels of conductivity [34]. Additionally, the conductivity exhibits a linear trend with temperature with activation energies of 1.19, 1.29, 0.78 and 1.33 eV for compositions x=0.05, 0.10, 0.15 and 0.20, respectively. In general, the conductivity increases with the samarium content, with the exception of $Bi_{0.85}Sm_{0.15}FeO_3$ that presents the lowest activation energy as well as the highest conductivity.

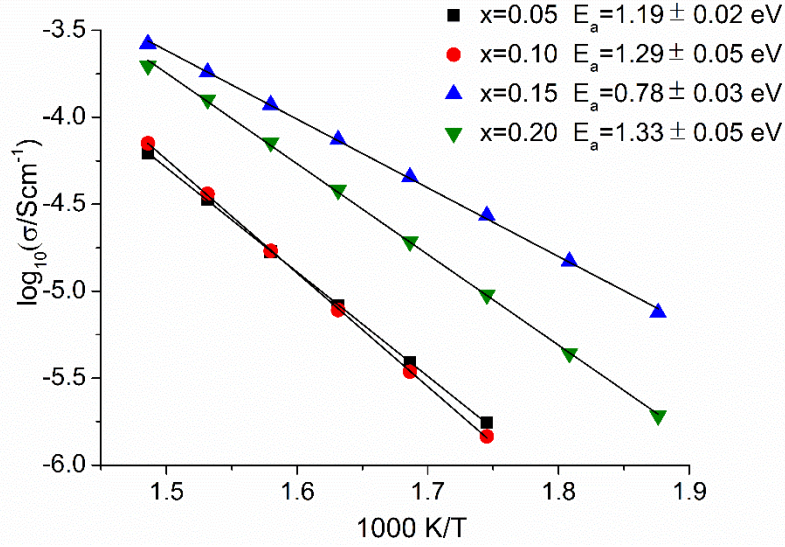Figure 11. Bulk conductivity data for $Bi_{1-x}Sm_xFeO_3$.

Magnetisation data from the $Bi_{1-x}Sm_xFeO_3$ samples were collected at the maximum temperature attained by the instrument (75 ºC), as a function of the applied field (Figure 12), with the objective of studying the magnetic properties above room temperature. The extracted parameters of the magnetisation data at 75ºC are presented in Table 4. The data show a modest increase in the remnant magnetisations of $Bi_{1-x}Sm_xFeO_3$ samples with samarium content up to a value of x = 0.10. There is a dramatic increase in M_r from the x = 0.15 sample, associated with a change to the Pbam structure. Thus, it can be seen that the samarium substitution does not dramatically increase the ferromagnetic moment of $Bi_{1-x}Sm_xFeO_3$ compositions in the ferroelectric compositional range.
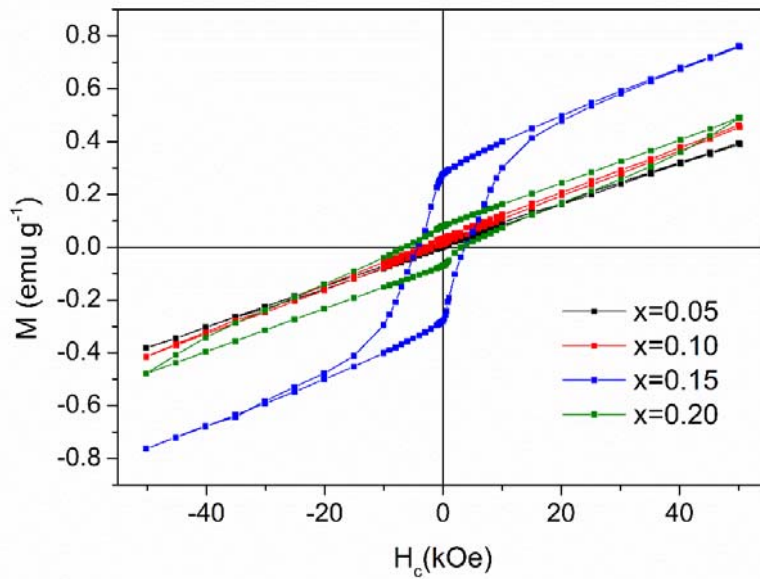

Figure 12. Magnetisation-field isotherms collected from $Bi_{1-x}Sm_xFeO_3$ samples at 75 ºC.

Table 4. Parameters extracted from the magnetisation data collected from $Bi_{1-x}Sm_xFeO_3$ at 75 ºC.

$Bi_{1-x}Sm_xFeO_3$	H_c (Oe)	M_r (emu mol^{-1})	M_r (emu g^{-1})	M_{5T} (emu g^{-1})
5	792	5.547	0.018	0.396
10	759	9.546	0.031	0.463
15	4028	101.599	0.334	0.762
20	4750	22.260	0.074	0.490

4. Discussion

Most published works describing the synthesis of bulk $Bi_{1-x}Sm_xFeO_3$ samples by several methods often report significant amounts of secondary phases, such as $Bi_2Fe_4O_9$ [29, 35-36, 47-53], most probably due to the high temperatures required for the synthesis that lead to bismuth deficiency and partial decomposition. In contrast, a close inspection of powder diffraction data, analysis via Rietveld refinement, TEM and EDX analysis demonstrates that the $Bi_{1-x}Sm_xFeO_3$ samples here prepared by mechanochemistry followed by sintering exhibit higher purity than those previously reported. Since the material was prepared by providing the reactants mechanical energy at room temperature, just a quick heating without annealing is enough for sintering, thereby preventing bismuth loss at high temperatures. Thus, in the case of the x = 0.05, 0.1, 0.15 and 0.2 compositions, the samples are, essentially, single phase, while two phases coexist in the case of the x = 0.125 and 0.175 compositions. These data highlight the importance of choosing an appropriate preparation method, which may be the reason of the large dispersion of data in the literature regarding the crystal structure as a function of the amount of samarium [13, 26, 31, 33, 54-56].

The two $Bi_{1-x}Sm_xFeO_3$ phases observed in the x = 0.125 and x = 0.175 samples can be considered an inherent feature of the $Bi_{1-x}Sm_xFeO_3$ chemical system, as such phase separation has been previously observed in other $Bi_{1-x}RE_xFeO_3$ samples [13, 26, 32, 57].

The phase diagram shown in Figure 9 is typical of rare earth substituted $BiFeO_3$ materials. Substitution of Bi for Sm drives an order/disorder structural transition, in which the ordered, polar displacement of the Bi^{3+} cations becomes disordered and ferroelectric behaviour is suppressed. The samarium concentration at which this occurs $0.1 < x < 0.15$ is consistent with observations made in other $Bi_{1-x}RE_xFeO_3$ systems [28]. Additionally, we confirm the hypothesis of previous studies about the high temperature paraelectric phase Pnma [13, 23].

The dielectric and magnetic behaviour of the $Bi_{1-x}Sm_xFeO_3$ $0 < x < 0.1$ samples change only modestly on Sm substitution, with neither a great increase in the resistivity or remnant magnetisation of the Sm substituted samples. Large changes are observed in the magnetisation and resistivity of samples when the level of samarium substitution drives a structural phase transition to the Pbam and Pnma phases ($x \geq 0.15$), however as ferroelectric behaviour is lost at this point these enhanced properties do not lead to improved magnetoelectric performance.

5. Conclusions

High-quality samples of composition $Bi_{1-x}Sm_xFeO_3$ ($0.05 < x < 0.2$) have been successfully prepared by direct mechanosynthesis. Pellets of the samples, sintered at 900ºC, present densities above 93% in all cases. Rietveld refinements demonstrate that, basically, single phase ceramics are obtained for x = 0.05, 0.1, 0.15 and 0.2 samples, and two phase mixtures for x = 0.125 and 0.175. Additionally, by a combination of the crystallographic information extracted by the Rietveld refinements, TEM, DSC, temperature-dependent DRX and permittivity data a tentative phase diagram has been constructed, were the presence of the high temperature Pnma phase has been confirmed for the $Bi_{1-x}Sm_xFeO_3$ system. Regarding the physical properties, the samples resulted to be electrically homogenous and highly insulating at room temperature, which is in contrast to many other previous reports. In spite of the high quality of the samples, the dielectric and magnetic behaviour of the $Bi_{1-x}Sm_xFeO_3$ samples change only modestly on Sm substitution, with neither a great change in the resistivity or remnant magnetisation of Sm substituted samples in comparison with $BiFeO_3$. Therefore, we can conclude that mechanochemical synthesis approaches allow the preparation of 'single-phase' $Bi_{1-x}RE_xFeO_3$ samples in which the possible amount of secondary phases is reduced to a minimum. The preparation of such samples allows the physical behaviour of the Sm substituted materials to be unambiguously measured and confirms that rare-earth substitution does not significantly improve the multiferroic performance of the host $BiFeO_3$ material.

6. Acknowledgements

7. References

[1]   Spaldin NA, Fiebig M. The renaissance of magnetoelectric multiferroics. Science 2005;309:391-392.

[2]   Eerenstein W, Mathur ND, Scott JF. Multiferroic and magnetoelectric materials. Nature 2006;442:759-765.

[3]   Cheong SW, Mostovoy M. Multiferroics: a magnetic twist for ferroelectricity. Nature Materials 2007;6:13-20.

[4]   Moreau JM, Michel C, Gerson R, James WJ. Ferroelectric $BiFeO_3$ X-ray and neutron diffraction study. Journal of Physics and Chemistry of Solids 1971;32:1315-1320.

[5]   Catalan G, Scott JF. Physics and Applications of Bismuth Ferrite. Advanced Materials 2009;21:2463-2485.

[6]   Selbach SM, Tybell T, Einarsrud M-A, Grande T. The ferroic phase transitions of $BiFeO_3$. Advanced Materials 2008;20:3692-3696.

[7]   Lu J, Qiao LJ, Fu PZ, Wu YC. Phase equilibrium of Bi_2O_3–Fe_2O_3 pseudo-binary system and growth of $BiFeO_3$ single crystal. Journal of Crystal Growth 2011;318:936-941.

[8]   Palai R, Katiyar RS, Schmid H, Tissot P, Clark SJ, Robertson J, Redfern SAT, Catalan G, Scott JF. beta phase and gamma-beta metal-insulator transition in multiferroic $BiFeO_3$. Physical Review B.

[9]   Roy A, Gupta R, Garg A. Multiferroic Memories. Advances in Condensed Matter Physics 2012;926290.

[10]   Zhang ST, Lu MH, Wu D, Chen YF, Ming NB. Larger polarization and weak ferromagnetism in quenched $BiFeO_3$ ceramics with a distorted rhombohedral crystal structure. Applied Physics Letters 2005;87:262907.

[11]   Maître A, François M, Gachon JC. Experimental study of the Bi_2O_3-Fe_2O_3 pseudo-binary system. Journal of Phase Equilibria and Diffusion 2004;25:59-67.

[12]   Perejon A, Sanchez-Jimenez PE, Criado JM, Perez-Maqueda LA. Thermal stability of multiferroic $BiFeO_3$: Kinetic nature of the beta-gamma transition and peritectic decomposition. Journal of Physical Chemistry C 2014;118:26387-26395.

[13]   Khodabakhsh M, Sen C, Khassaf H, Gulgun MA, Misirlioglu IB. Strong smearing and disappearance of phase transitions into polar phases due to inhomogeneous lattice

strains induced by A-site doping in $Bi_{(1-x)}A_{(x)}FeO_{(3)}$ (A: La, Sm, Gd). Journal of Alloys and Compounds 2014;604:117-129.

[14]   Morozov MI, Lomanova NA, Gusarov VV. Specific features of $BiFeO_3$ formation in a mixture of bismuth(III) and iron(III) oxides. Russian Journal of General Chemistry 2003;73:1676-1680.

[15]   Valant M, Axelsson AK, Alford N. Peculiarities of a solid-state synthesis of multiferroic polycrystalline $BiFeO_3$. Chemistry of Materials 2007;19:5431-5436.

[16]   Selbach SM, Einarsrud MA, Grande T. On the thermodynamic stability of $BiFeO_3$. Chemistry of Materials 2009;21:169-173.

[17]   Arya GS, Sharma RK, Negi NS. Enhanced magnetic properties of Sm and Mn co-doped $BiFeO_3$ nanoparticles at room temperature. Materials Letters 2013;93:341-344.

[18]   Gonzalez Garcia F, Riccardi CS, Simões AZ. Lanthanum doped $BiFeO_3$ powders: Syntheses and characterization. Journal of Alloys and Compounds 2010;501:25-29.

[19]   Rai R, Mishra SK, Singh NK, Sharma S, Kholkin AL. Preparation, structures, and multiferroic properties of single-phase $BiRFeO_3$, R = La and Er ceramics. Current Applied Physics 2011;11:508-512.

[20]   Mishra RK, Pradhan DK, Choudhary RNP, Banerjee A. Effect of yttrium on improvement of dielectric properties and magnetic switching behavior in $BiFeO_3$. Journal of Physics-Condensed Matter 2008;20:045218.

[21]   Yao YB, Liu WC, Mak CL. Pyroelectric properties and electrical conductivity in samarium doped $BiFeO_3$ ceramics. Journal of Alloys and Compounds 2012;527:157-162.

[22]   Singh H, Yadav KL. Structural, dielectric, vibrational and magnetic properties of Sm doped $BiFeO_3$ multiferroic ceramics prepared by a rapid liquid phase sintering method. Ceramics International 2015;41:9285-9295.

[23]   Karimi S, Reaney IM, Han Y, Pokorny J, Sterianou I. Crystal chemistry and domain structure of rare-earth doped $BiFeO_3$ ceramics. Journal of Materials Science 2009;44:5102-5112.

[24]   Rusakov DA, Abakumov AM, Yamaura K, Belik AA, Van Tendeloo G, Takayama-Muromachi E. Structural evolution of the $BiFeO_3$-$LaFeO_3$ system. Chemistry of Materials 2011;23:285-292.

[25]   Maso N, West AR. Electrical properties of Ca-doped $BiFeO_3$ ceramics: From p-type semiconduction to oxide-ion conduction. Chemistry of Materials 2012;24:2127-2132.

[26]   Khomchenko VA, Paixao JA, Costa BFO, Karpinsky DV, Kholkin AL, Troyanchuk IO, Shvartsman VV, Borisov P, Kleemann W. Structural, ferroelectric and magnetic properties of $Bi_{0.85}Sm_{0.15}FeO_3$ perovskite. Crystal Research and Technology 2011;46:238-242.

[27]   Khomchenko VA, Paixão JA, Kiselev DA, Kholkin AL. Intermediate structural phases in rare-earth substituted $BiFeO_3$. Materials Research Bulletin 2010;45:416-419.

[28]   Arnold DC. Composition-Driven Structural Phase Transitions in Rare-Earth-Doped $BiFeO_3$ Ceramics: A Review. Ieee Transactions on Ultrasonics Ferroelectrics and Frequency Control 2015;62:62-82.

[29] Yan Z, Wang KF, Qu JF, Wang Y, Song ZT, Feng SL. Processing and properties of Yb-doped $BiFeO_3$ ceramics. Applied Physics Letters 2007;91:082906.

[30] Nalwa KS, Garg A, Upadhyaya A. Effect of samarium doping on the properties of solid-state synthesized multiferroic bismuth ferrite. Materials Letters 2008;62:878-881.

[31] Pattanayak S, Choudhary RNP, Das P. Effect of Sm-substitution on structural, electrical and magnetic properties of $BiFeO_3$. Electronic Materials Letters 2014;10:165-172.

[32] Walker J, Bryant P, Kurusingal V, Sorrell C, Kuscer D, Drazic G, Bencan A, Nagarajan V, Rojac T. Synthesis-phase-composition relationship and high electric-field-induced electromechanical behavior of samarium-modified $BiFeO_3$ ceramics. Acta Materialia 2015;83:149-159.

[33] Khomchenko VA, Paixao JA, Shvartsman VV, Borisov P, Kleemann W, Karpinsky DV, Kholkin AL. Effect of Sm substitution on ferroelectric and magnetic properties of $BiFeO_3$. Scripta Materialia 2010;62:238-241.

[34] Godara P, Agarwal A, Ahlawat N, Sanghi S. Crystal structure refinement, dielectric and magnetic properties of Sm modified $BiFeO_3$ multiferroic. Journal of Molecular Structure 2015;1097:207-213.

[35] Nalwa KS, Garg A. Phase evolution, magnetic and electrical properties in Sm-doped bismuth ferrite. Journal of Applied Physics 2008;103:044101.

[36] Iorgu AI, Maxim F, Matei C, Ferreira LP, Ferreira P, Cruz MM, Berger D. Fast synthesis of rare-earth (Pr^{3+}, Sm^{3+}, Eu^{3+} and Gd^{3+}) doped bismuth ferrite powders with enhanced magnetic properties. Journal of Alloys and Compounds 2015;629:62-68.

[37] Perejon A, Sanchez-Jimenez PE, Perez-Maqueda LA, Criado JM, de Paz JR, Saez-Puche R, Maso N, West AR. Single phase, electrically insulating, multiferroic La-substituted $BiFeO_3$ prepared by mechanosynthesis. Journal of Materials Chemistry C 2014;2:8398-8411.

[38] Perejon A, Murafa N, Sanchez-Jimenez PE, Criado JM, Subrt J, Dianez MJ, Perez-Maqueda LA. Direct mechanosynthesis of pure $BiFeO_3$ perovskite nanoparticles: reaction mechanism. Journal of Materials Chemistry C 2013;1:3551-3562.

[39] Perejon A, Maso N, West AR, Sanchez-Jimenez PE, Poyato R, Criado JM, Perez-Maqueda LA. Electrical Properties of Stoichiometric $BiFeO_3$ Prepared by Mechanosynthesis with Either Conventional or Spark Plasma Sintering. Journal of the American Ceramic Society 2013;96:1220-1227.

[40] Perejon A, Gil-Gonzalez E, Sanchez-Jimenez PE, Criado JM, Perez-Maqueda LA. Structural, Optical, and Electrical Characterization of Yttrium-Substituted $BiFeO_3$ Ceramics Prepared by Mechanical Activation. Inorganic Chemistry 2015;54:9876-9884.

[41] Da Silva KL, Menzel D, Feldhoff A, Kubel C, Bruns M, Paesano A, Duvel A, Wilkening M, Ghafari M, Hahn H, Litterst FJ, Heitjans P, Becker KD, Sepelak V. Mechanosynthesized $BiFeO_3$ Nanoparticles with Highly Reactive Surface and Enhanced Magnetization. Journal of Physical Chemistry C 2011;115:7209-7217.

[42]   Freitas VF, Grande HLC, de Medeiros SN, Santos IA, Cotica LF, Coelho AA. Structural, microstructural and magnetic investigations in high-energy ball milled $BiFeO_3$ and $Bi_{0.95}Eu_{0.05}FeO_3$ powders. Journal of Alloys and Compounds 2008;461:48-52.

[43]   Moure A, Tartaj J, Moure C. Processing and characterization of Sr doped $BiFeO_3$ multiferroic materials by high energetic milling. Journal of Alloys and Compounds 2011;509:7042-7046.

[44]   Gil-Gonzalez E, Perejon A, Sanchez-Jimenez PE, Hayward MA, Perez-Maqueda LA. Preparation of ytterbium substituted BiFeO3 multiferroics by mechanical activation. Journal of the European Ceramic Society 2017;37:945-954.

[45]   Arnold DC, Knight KS, Morrison FD, Lightfoot P. Ferroelectric-Paraelectric Transition in $BiFeO_3$: Crystal Structure of the Orthorhombic beta Phase. Physical Review Letters 2009;102:027602.

[46]   Jonsher AK, *Universal relaxation law*, Chelsea Dielectric Press, London, 1996.

[47]   Sharma P, Satapathy S, Varshney D, Gupta PK. Effect of sintering temperature on structure and multiferroic properties of $Bi_{0.825}Sm_{0.175}FeO_3$ ceramics. Materials Chemistry and Physics 2015;162:469-476.

[48]   Dai H, Chen Z, Xue R, Li T, Liu H, Wang Y. Structure and multiferroic properties of Eu-substituted $BiFeO_3$ ceramics. Applied Physics A 2013;111:907-912.

[49]   Sati PC, Kumar M, Chhoker S, Jewariya M. Influence of Eu substitution on structural, magnetic, optical and dielectric properties of $BiFeO_3$ multiferroic ceramics. Ceramics International 2015;41:2389-2398.

[50]   Dhanalakshmi R, Muneeswaran M, Shalini K, Giridharan NV. Enhanced photocatalytic activity of La-substituted $BiFeO_3$ nanostructures on the degradation of phenol red. Materials Letters 2016;165:205-209.

[51]   Jia D-C, Xu J-H, Ke H, Wang W, Zhou Y. Structure and multiferroic properties of $BiFeO_3$ powders. Journal of the European Ceramic Society 2009;29:3099-3103.

[52]   Yan X, Chen J, Qi Y, Cheng J, Meng Z. Hydrothermal synthesis and characterization of multiferroic $Bi_{1-x}La_xFeO_3$ crystallites. Journal of the European Ceramic Society 2010;30:265-269.

[53]   Luo L, Wei W, Yuan X, Shen K, Xu M, Xu Q. Multiferroic properties of Y-doped $BiFeO_3$. Journal of Alloys and Compounds 2012;540:36-38.

[54]   Dai HY, Chen ZP, Li T, Li Y. Microstructure and properties of Sm-substituted $BiFeO_3$ ceramics. Journal of Rare Earths 2012;30:1123-1128.

[55]   Arora M, Kumar M. Electron spin resonance probed enhanced magnetization and optical properties of Sm doped $BiFeO_3$ nanoparticles. Materials Letters 2014;137:285-288.

[56]   Chen XM, Wang JL, Yuan GL, Wu D, Liu JM, Yin J, Liu ZG. Structure, ferroelectric and piezoelectric properties of multiferroic $Bi_{0.875}Sm_{0.125}FeO_3$ ceramics. Journal of Alloys and Compounds 2012;541:173-176.

[57]   Alikin DO, Turygin AP, Walker J, Rojac T, Shvartsman VV, Shur VY, Kholkin AL. Quantitative phase separation in multiferroic $Bi_{0.88}Sm_{0.12}FeO_3$ ceramics via piezoresponse force microscopy. Journal of Applied Physics 2015;118:072004.